Competition between Coulomb and symmetry potential in semi-peripheral heavy ion collisions

Qianghua Wu (吴强华),[1,2] Yingxun Zhang (张英逊),[1,*] Zhigang Xiao (肖志刚),[3,4] Rensheng Wang (王仁生),[3] Yan Zhang (张嫣),[3] Zhuxia Li (李祝霞),[1] Ning Wang (王宁),[2] and R. H. Showalter[5,6]

[1]*China Institute of Atomic Energy, Beijing 102413, China*

[2]*Department of Physics and Technology, Guangxi Normal University, Guilin 541004, China*

[3]*Department of Physics, Tsinghua University, Beijing 100084, China*

[4]*Collaborative Innovation Center of Quantum Matter, Beijing 100084, China*

[5]*National Superconducting Cyclotron Laboratory, Michigan State University, East Lansing, Michigan 48864, USA*

[6]*Department of Physics and Astronomy, Michigan State University, East Lansing, Michigan 48864, USA*

(Received 28 September 2014; revised manuscript received 1 December 2014; published 30 January 2015)

The anisotropy of angular distributions of emitted nucleons and light charged particles for the asymmetric reaction system ^{40}Ar + ^{197}Au, at $b = 6$ fm and $E_{\rm beam} = 35, 50$, and 100 MeV/nucleon, is investigated by using the improved quantum molecular dynamics model. The competition between the symmetry potential and Coulomb potential shows large impacts on the nucleons and light charged particles emission in the projectile and target region. As a result of this competition, the angular distribution anisotropy of coalescence invariant neutron to proton yield ratio at forward regions shows sensitivity to the stiffness of symmetry energy as well as the value of neutron to proton yield ratio. This observable can be further checked against experimental data to understand the reaction mechanism and to extract information about the symmetry energy at subsaturation densities.

DOI: 10.1103/PhysRevC.91.014617 PACS number(s): 21.65.Ef, 24.10.Lx, 25.70.−z, 02.70.Ns

I. INTRODUCTION

Nuclear symmetry energy plays a crucial role in understanding not only nuclear structures and reactions but also astrophysical phenomena. However, theoretical predictions for the density dependence of the symmetry energy of nuclear matter show large uncertainties away from the normal density [1,2]. Many efforts have been devoted to probe and constrain the symmetry energy at both subsaturation and suprasaturation densities by analyzing observables from nuclear reactions, nuclear structures, and neutron stars, such as isospin diffusion [3–9], double neutron to proton ratio (DR(n/p)) [10–17], light charged particle flow [18–23], π^-/π^+ [24–28], neutron skin [29–31], giant dipole resonance and pygmy dipole resonance [32–34] and masses of isospin analog state [35], α decay [36], the mass-radius relationship, and gravitational waves from merging neutron star binaries [37,38]. Up to now, a consensus on the constraints of symmetry energy at subsaturation density [39,40] has been obtained. Nevertheless, differences among the constraints of the symmetry energy obtained from different models or approaches still exist. Understanding these differences is a challenge in this field and stimulates nuclear physicists to propose new probes that are sensitive enough to further discriminate the stiffness of symmetry energy and to perform new experiments for a comprehensive understanding of the mechanism of neutron-rich heavy ion collisions.

Some probes related to the slower reaction process for semi-peripheral collisions in asymmetric reaction systems near the Fermi energy have been investigated or measured to understand the reaction mechanism of neutron-rich heavy ion collisions (HICs) and to extract information about the symmetry energy [41–45]. For example, in Ref. [41], the isotopic composition of intermediate mass fragments (IMFs) emitted at midrapidity in semi-peripheral collisions of ^{124}Sn + ^{64}Ni was analyzed and it was found that the IMFs emitted in the early stage of the reaction show larger values of $\langle N/Z\rangle$ and stronger angular anisotropy. The linear density dependence of the symmetry energy was obtained by comparing the data with the stochastic mean field (SMF) model. Calculations from the transport model [46] also show that the dynamical emission of nucleons and light charged particles (LCPs) for asymmetric reaction systems, such as $Y(n)/Y(p)$ ratios and $Y(t)/Y(^3\mathrm{He})$ ratios as a function of impact parameters, is also sensitive to the density dependence of the symmetry energy due to the isospin migration and diffusion mechanism in the neck region. Very recently, R. S. Wang *et al.* analyzed the energy spectra of light charged particles in coincidence with fission fragments in ^{40}Ar + ^{197}Au at 35 MeV/nucleon [44]. The triggering condition on fission events in experiment has a bias on the semi-peripheral collisions. By defining the ratio of the isotopic yield (normalized to that of a proton) at 80° and 158°, $R_{\rm iso}(X) = (\frac{[Y(X)/Y(p)]_{80}}{[Y(X)/Y(p)]_{158}})$, where X represents all species with $Z = 1$ and 2, it is found that $R_{\rm iso}$ increases with N/Z of the species, indicating a relatively high neutron richness of the emitted particles at smaller angle. According to the studies in Ref. [47], this result can be attributed to the hierarchical feature of the semi-peripheral collisions at Fermi energies, saying that the heavier fragments are faster than the lighter fragments along the beam direction and the Coulomb potential is stronger near the projectile or target region compared to that at midrapidities. Thus, one can expect different $Y(n)/Y(p)$ ratio at project or target region and midrapidities, naturally leading to a nonunity value of $R_{\rm iso}$. The different form of the symmetry energy may lead to different values of anisotropy of isospin contents, $R_{\rm iso}(X) = R_X(\theta 1)/R_X(\theta 2)$, in the simulations. Furthermore, the nonunity value of $R_{\rm iso}$ also suggests the reaction process is a nonequilibrium process. An

*zhyx@ciae.ac.cn

investigation on angular distribution of the N/Z of the light particles may reveal the sequence of the particle emission with different isospin composition, which carries the information of the symmetry energy at subsaturation densities.

In this work, we mainly discuss the dynamical emission of nucleons and LCPs at early stages for the asymmetric nuclear reaction system ^{40}Ar + ^{197}Au at semi-peripheral collisions by using the IMQMD05 code. In our simulations, the beam energy dependence of the angular distribution of the coalescence invariant neutron-to-proton ratios is also discussed from 35 to 100 MeV/nucleon. Based on our calculations, we propose that the anisotropy of the angular distribution of the coalescence invariant neutron-to-proton ratios may be used to understand the competition between the Coulomb and symmetry potential, and it may be used for probing the isospin effects and the form of the symmetry energy.

II. BRIEF INTRODUCTION OF IMPROVED QUANTUM MOLECULAR DYNAMICS MODEL

Within the improved quantum molecular dynamics model (IMQMD05 code) [12,48,49], nucleons are represented by Gaussian wave packets, and the mean fields acting on these wave packets are derived from an energy density functional with the potential energy U that includes the Skyrme potential energy with just the spin-orbit term omitted:

$$U = U_\rho + U_{\rm md} + U_{\rm Coul} \tag{1}$$

where U_ρ is the Skyrme potential energy, $U_{\rm md}$ is the momentum dependent potential energy, and $U_{\rm Coul}$ is the Coulomb energy. The nuclear contributions are represented in a local form with

$$U_{\rho,{\rm md}} = \int u_{\rho,{\rm md}}\, d^3r \tag{2}$$

and

$$u_\rho = \frac{\alpha}{2}\frac{\rho^2}{\rho_0} + \frac{\beta}{\eta+1}\frac{\rho^{\eta+1}}{\rho_0^\eta} + \frac{g_{\rm sur}}{2\rho_0}(\nabla\rho)^2 + \frac{g_{\rm sur,iso}}{\rho_0}[\nabla(\rho_n-\rho_p)]^2 + \frac{C_s}{2}\left(\frac{\rho}{\rho_0}\right)^{\gamma_i}\delta^2\rho + g_{\rho\tau}\frac{\rho^{8/3}}{\rho_0^{5/3}}. \tag{3}$$

Here, $\delta = (\rho_n-\rho_p)/(\rho_n+\rho_p)$ is the isospin asymmetry, and ρ_n, ρ_p are the neutron and proton densities, respectively. A symmetry potential energy density of the form $\frac{C_s}{2}(\rho/\rho_0)^{\gamma_i}\delta^2\rho$ is used in the following calculations. The energy density associated with the mean-field momentum dependence is represented by

$$u_{\rm md} = \frac{1}{2\rho_0}\sum_{N1}\frac{1}{16\pi^6}\int d^3p_1 d^3p_2 f_{N1}(\vec{p}_1) f_{N2}(\vec{p}_2) 1.57 \times [\ln(1+5\times10^{-4}(\Delta p)^2)]^2, \tag{4}$$

where f_N are nucleon phase space distribution functions, $\Delta p = |\vec{p}_1 - \vec{p}_2|$, the energy is in MeV and momenta are in MeV/nucleon. The resulting interaction between wave packets is described in Ref. [50]. In this work, $\alpha = -356$ MeV, $\beta = 303$ MeV, $\eta = 7/6$, $g_{\rm sur} = 19.47$ MeV fm^2, $g_{\rm sur,iso} = -11.35$ MeV fm^2, $C_s = 35.19$ MeV, and $g_{\rho,\tau} = 0$ MeV. The fragments are recognized by the isospin dependent minimum spanning tree method [51].

III. RESULTS AND DISCUSSION

In this section, we examine the competition between the different forms of symmetry potential and Coulomb potential for peripheral collisions for ^{40}Ar + ^{197}Au by using the IMQMD model. The time evolution of the density, symmetry potential, and single particle potential felt by the neutron and proton at the overlapped region are analyzed. The competition can be clearly observed at the projectile and target region, which leads to the different values of anisotropy of angular distribution of light particles for different forms of symmetry potential.

A. Reaction dynamics and time evolution of $V^q_{\rm sym}$ and V_q at neck region

Figure 1 shows the density contour plots for the ^{40}Ar + ^{197}Au reaction at a beam energy of 35 MeV/nucleon and impact parameter $b = 6$ fm. In the calculations, the projectile and target start to touch at around 50 fm/c, and then the overlapped region is formed and it reaches maximum compression at around 90 fm/c. After about 150 fm/c, the overlapped region expands to lower density and ruptures into fragments. For the semi-peripheral collisions we studied, the neck dynamics plays an important role in the dynamical emission of LCPs [52], and its yields and isospin contents for nucleons and LCPs are closely related to the symmetry potential in the participant region of the reaction. Thus, it is useful for us to understand how the symmetry potential and single particle potential for neutrons and protons in the participant region evolve with time, because the single particle potential and symmetry potential will determine the yields and isospin contents of nucleons and LCP emission.

Figure 2(a) shows the time evolution of the symmetry potential $V^q_{\rm sym} = \frac{C_s}{2}[(\gamma_i-1)u^{\gamma_i}\delta^2 \pm 2u^{\gamma_i}\delta]$, where $u = \rho/\rho_0$, $q = n, p$, at the overlapped region which is presented as blue points in Fig. 1. The point is defined as the equal distance from the surface of the projectile and the target, and a spherical region with twice the nucleon radius, i.e., $R = 1.7$ fm, is used to approximately describe the center of the overlapped region in the calculations. The solid lines are the results from $\gamma_i = 0.5$ and dashed lines are for $\gamma_i = 2.0$. The magnitude of the symmetry potential felt by the neutron ($V^n_{\rm sym}$) for $\gamma_i = 0.5$ is obviously larger than that for $\gamma_i = 2.0$ except for the time at around 80 fm/c, where $V^n_{\rm sym}(\gamma_i = 0.5) < V^n_{\rm sym}(\gamma_i = 2.0)$. The reason is that the compressed density is close and up to normal density at around 80 fm/c, and its isospin asymmetry comes close to 0.2 due to isospin migration. Thus, the symmetry potential felt by the neutron ($V^n_{\rm sym}$) obtained with $\gamma_i = 2.0$ becomes larger than that for $\gamma_i = 0.5$ at $\rho > 0.9\rho_0$ based on the formula of $V^q_{\rm sym}$ [46,53]. However, the magnitude of the symmetry potential felt by the proton for $\gamma_i = 2.0$ is still smaller than that for $\gamma_i = 0.5$ at $\rho \leqslant 1.1\rho_0$ for $\delta \sim 0.2$, and it leads to the larger magnitude of the symmetry potential felt by the proton for $\gamma_i = 0.5$ than that for $\gamma_i = 2.0$ at different time for the beam energy of 35 MeV/nucleon. Since HIC

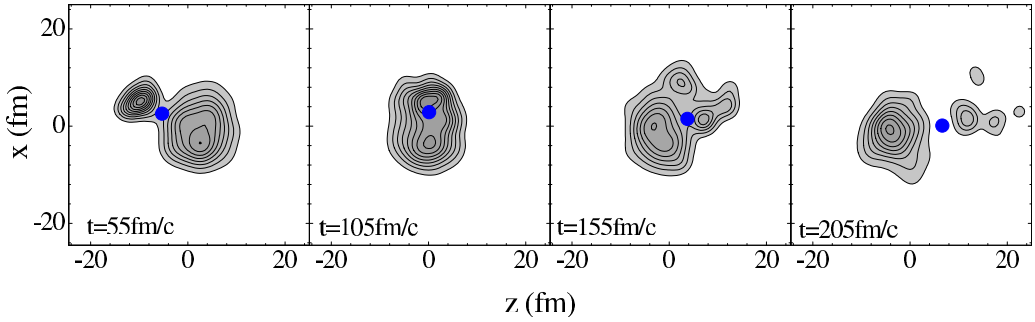

FIG. 1. (Color online) Time evolution of the density contour plots in the reaction plane for ^{40}Ar + ^{197}Au collisions at $E_{\rm beam}$ = 35 MeV/nucleon and b = 6 fm from one typical event; the blue points represent the center of overlapped region of projectile and target.

observables obtained in the simulations are determined by the reaction process from early stages to late stages, one can expect that the yield ratio of neutron to proton, i.e., $Y(n)/Y(p)$, obtained with $\gamma_i = 0.5$ is greater than that with $\gamma_i = 2.0$ for a neutron rich reaction system. Quantitatively, understanding the $Y(n)/Y(p)$ ratios requires knowledge of the single particle potential felt by neutrons and protons in the reaction system. Figures 2(b) and 2(c) show the single particle potential for neutrons and protons for $\gamma_i = 0.5$ and 2.0, respectively. The solid lines are for protons where the Coulomb contribution is included; i.e., $V_p + V_{\rm Coul}$. The dashed lines are the nucleonic potential felt by the proton, i.e., V_p, without the Coulomb potential. The dotted lines are the single particle potential for neutrons, i.e., V_n. Figure 2(b) shows that $V_p + V_{\rm Coul}$ is close to V_n for $\gamma_i = 0.5$. However, for $\gamma_i = 2.0$, $V_p + V_{\rm Coul}$ is obviously larger than V_n after 120 fm/c because the symmetry potential becomes weak, especially at lower density. Thus, the Coulomb potential obviously moves the single particle potential felt by the proton up to the strength of that felt by the neutron. It may lead to a higher yield for protons than for neutrons, if the Coulomb repulsion is strong enough. Especially for asymmetric reaction systems at semi-peripheral collisions, one can expect to observe this competition between the Coulomb and symmetry potentials which influences the isospin contents for the emitted nucleons and LCPs; hence, their angular distribution anisotropies show sensitivity to the different forms of symmetry energy.

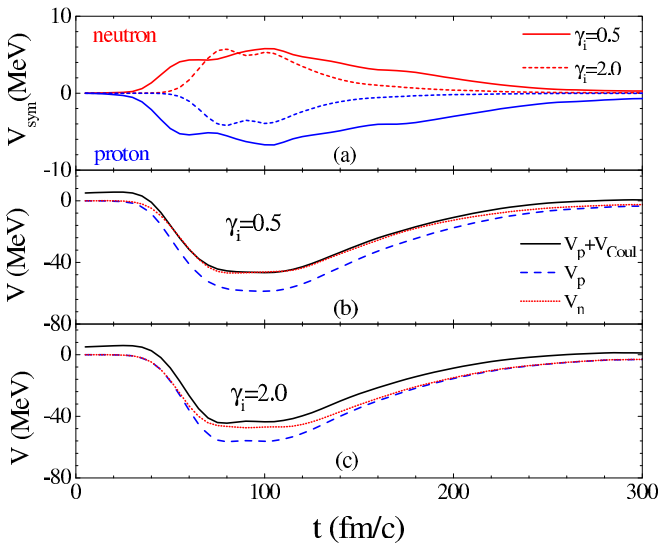

FIG. 2. (Color online) (a) Time evolution of the symmetry potential for neutrons and protons obtained with $\gamma_i = 0.5$ (solid lines) and 2.0 (dashed lines); single particle potential for neutron and proton for (b) $\gamma_i = 0.5$ and (c) $\gamma_i = 2.0$ at the overlapped region for ^{40}Ar + ^{197}Au at b = 6 fm and $E_{\rm beam}$ = 35 MeV/nucleon.

B. Angular distribution of the coalescence invariant yields for neutrons and protons

As is known, the absolute yields of LCPs are not very well reproduced due to the considerable deviation of the binding energy of light clusters between the quantum molecular dynamics (QMD) model and experimental data [54]. Loosely bound clusters like d, t are overpredicted, whereas strongly bound clusters like ^{4}He are underpredicted due to their lower binding energy in the QMD model. Therefore, it is hard to draw a firm conclusion by comparing the absolute number of these light fragments to data to extract information about physical quantities such as the equation of state. One method to eliminate the problem related to the absolute yield of LCPs is to introduce the coalescence invariant neutron and proton yields and to construct the related observables, such as coalescence invariant $Y(n)/Y(p)$ (CI n/p) ratio spectra [11,12,55]. In this paper, we investigate the angular distributions of the CI n/p ratio by varying the stiffness of the symmetry potential. The angular distribution of CI neutron and proton yields are constructed by adding the neutrons and protons in light particles to free neutrons and protons at given $\theta_{\rm c.m.}$ as follows:

$$\frac{dM_{n,\rm CI}}{d\theta_{\rm c.m.}} = \sum_{N,Z} N \frac{dY(N,Z)}{d\theta_{\rm c.m.}}, \tag{5}$$

$$\frac{dM_{p,\rm CI}}{d\theta_{\rm c.m.}} = \sum_{N,Z} Z \frac{dY(N,Z)}{d\theta_{\rm c.m.}}, \tag{6}$$

the summation is over n, p, d, t, ^{3}He, ^{4}He, and ^{6}He in this work, and $Y(N,Z)$ is the yield of fragments with charge number Z and neutron number N.

To understand the origin of the angular distribution of CI yields for neutrons and protons in asymmetric reaction systems ^{40}Ar + ^{197}Au at 35 MeV/nucleon, we show the angular distribution of the yields for CI neutrons and CI

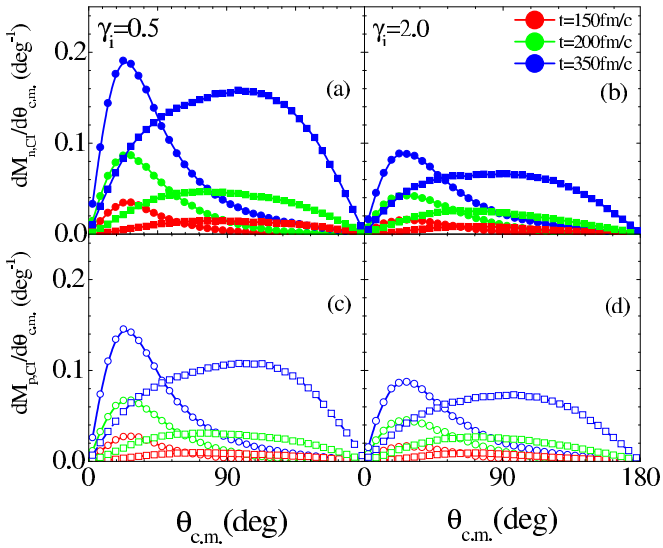

FIG. 3. (Color online) The angular distribution of the yields for (a, b) CI neutrons and (c, d) CI protons emitted from a projectile (line with circle symbols, left curves in each panel) or a target (line with square symbols, right curves in each panel) at 150, 200, and 350 fm/c; (a, c) $\gamma_i = 0.5$ and (b, d) $\gamma_i = 2.0$.

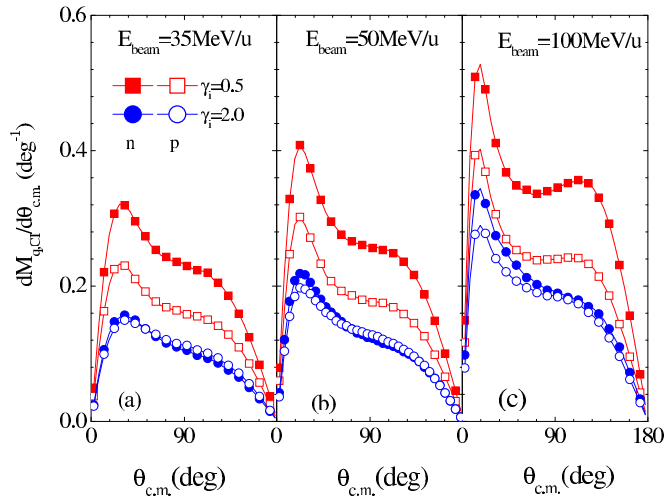

FIG. 4. (Color online) Angular distribution of the yields for CI neutrons (solid symbols) and CI protons (open symbols) emitted at $t = 400$ fm/c obtained with $\gamma_i = 0.5$ (red symbols) and $\gamma_i = 2.0$ (blue symbols). Left: result at the beam energy of 35 MeV/nucleon; middle: result for 50 MeV/nucleon; right: result for 100 MeV/nucleon. The impact parameter is 6 fm.

protons emitted from the projectile (line with circles) and the target (line with squares) at 150, 200, and 350 fm/c in Fig. 3. Figures 3(a) and 3(c) show the results for $\gamma_i = 0.5$, and Figs. 3(b) and 3(d) are for $\gamma_i = 2.0$. The line with open (solid) symbols refers to the yields of CI protons in Figs. 3(c) and 3(d) [CI neutrons are in Figs. 3(a) and 3(b)]. The calculated results show that the yields of CI nucleons from the target have a wide angular distribution and exhibit weak anisotropy in the angular distributions. The peak of the angular distribution appears below $\theta_{\mathrm{c.m.}} \sim 90^\circ$ when the time is earlier than ~300 fm/c; i.e., the nucleons and LCPs prefer to emit at forward regions for asymmetric reaction systems because the neck dynamics dominates the nucleons' and LCPs' emission at earlier stages. After that, the peak moves to the backward regions at late stages because the evaporation from targetlike fragments becomes more and more important. The yields of CI nucleons from the projectile obviously peak around $\theta_{\mathrm{c.m.}} \sim 25^\circ$ and the corresponding angular position does not obviously vary with time. As shown in Fig. 3, the nucleons emitted at $\theta_{\mathrm{c.m.}} < 25^\circ$ are mainly from the projectile whereas those at $\theta_{\mathrm{c.m.}} > 60^\circ$ are mainly from the target. The emission of nucleons within the angular gate $20^\circ < \theta_{\mathrm{c.m.}} < 60^\circ$ corresponds to the compressed overlap region between the projectile and target. The anisotropy of the angular distribution of CI nucleons is due to the asymmetry of the projectile and target in semi-peripheral collisions. Furthermore, one also observes that the yields of neutrons are obviously larger than that for protons after 150 fm/c for $\gamma_i = 0.5$. But for $\gamma_i = 2.0$, the yields of protons from the target are always higher than that for neutrons when $\theta_{\mathrm{c.m.}} > 60^\circ$. The reason is that the strength of the symmetry potential is weak for $\gamma_i = 2.0$ at low density regions where many nucleons are emitted, and the targetlike fragments provide stronger Coulomb repulsion. Thus, the yields of protons become larger than that for neutrons for $\gamma_i = 2.0$. For the nucleons from the projectile, one also observes that yields of protons are greater than neutrons before 300 fm/c, but it finally turns over. After 300 fm/c, the yields of protons and neutrons become similar because of the weaker Coulomb potential in the projectile region.

Figure 4(a) shows the angular distributions of yields of CI neutrons (solid symbols) and protons (open symbols) for $\gamma_i = 0.5$ (red squares) and $\gamma_i = 2.0$ (blue circles) at the stop time of simulations, $t = 400$ fm/c, for $E_{\mathrm{beam}} = 35$ MeV/nucleon and $b = 6$ fm. In general, the yields of nucleons obtained with $\gamma_i = 0.5$ are greater than that for $\gamma_i = 2.0$ due to its stronger symmetry energy at subsaturation densities. For the isospin contents, the yields of neutrons are always greater than the yields of protons at whole angular range for $\gamma_i = 0.5$. Similar to the results at 35 MeV/nucleon, the yields of neutrons are greater than that for protons for the beam energy at 50 [Fig. 4(b)] and 100 MeV/nucleon [Fig. 4(c)]. But for $\gamma_i = 2.0$, a different behavior appears in the yields of neutrons and protons. At the beam energy of 35 MeV/nucleon, the yields of neutrons become a little bit less than the yields of protons at $\theta_{\mathrm{c.m.}} > 60^\circ$ for $\gamma_i = 2.0$. It is the result of the competition between the Coulomb potential and the symmetry potential for an asymmetric reaction system at semi-peripheral collisions, as mentioned before. At the beam energy of 100 MeV/nucleon, the reaction is more violent and a larger part of the colliding system is dissociated into gases (nucleons and light particles), and thus more neutrons originally bound in the system are released and outnumber the protons for the whole angular region, as shown in Fig. 4(c).

C. Correlation between the symmetry energy and angular distribution of CI n/p ratios

Consequently, we construct the angular distribution of CI n/p ratios, i.e., $\frac{dM_{n,\mathrm{CI}}}{d\theta_{\mathrm{c.m.}}} / \frac{dM_{p,\mathrm{CI}}}{d\theta_{\mathrm{c.m.}}}$ ratios, to explore the information

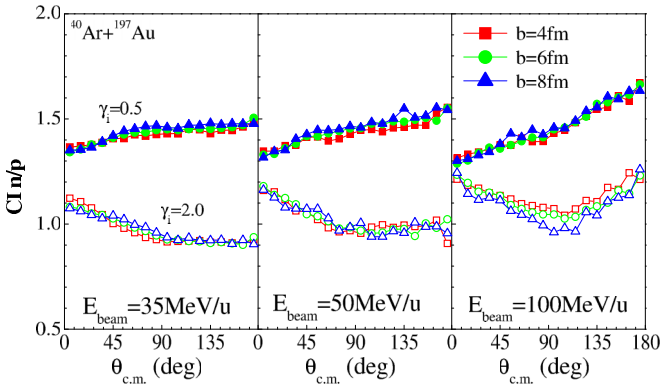

FIG. 5. (Color online) Left: calculated results for CI n/p ratios as a function of $\theta_{\mathrm{c.m.}}$ for $b = 4$, 6, and 8 fm at $E_{\mathrm{beam}} = 35$ MeV/nucleon. The solid symbols are for $\gamma_i = 0.5$ and open symbols are for $\gamma_i = 2.0$. Middle: results for 50 MeV/nucleon; right: results for 100 MeV/nucleon.

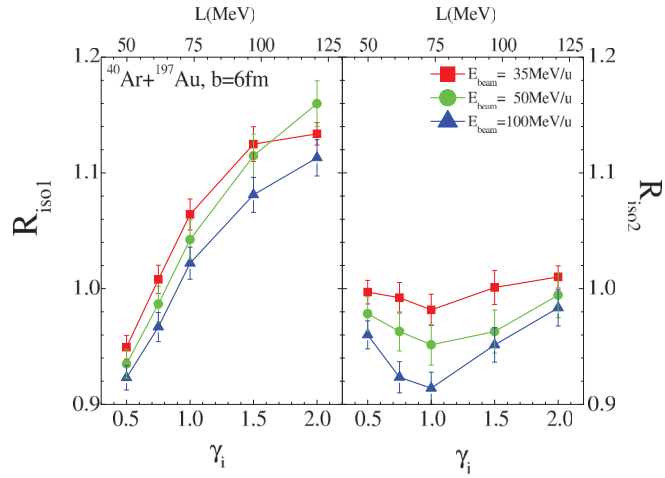

FIG. 6. (Color online) The calculated results of R_{iso1} (left) and R_{iso2} (right) as a function of γ_i for ^{40}Ar + ^{197}Au at $b = 6$ fm and beam energy 35, 50, and 100 MeV/nucleon.

of the reaction mechanism and symmetry energy. As shown in Fig. 5, the CI n/p ratios obtained with $\gamma_i = 0.5$ are greater than that obtained with $\gamma_i = 2.0$ for the beam energy we studied, because the symmetry energy for $\gamma_i = 0.5$ is stronger than that for $\gamma_i = 2.0$ at subsaturation density. The sensitivity of CI n/p ratios to γ_i becomes large at the region where the emitted fragments with large charge number. It is consistent with the results in Ref. [56], where the influence of the symmetry potential and in-medium nucleon-nucleon cross section on the free nucleon n/p ratio were studied for the central collision of ^{100}Zn + ^{40}Ca at 200 MeV/nucleon.

In addition to the values of the CI n/p ratio, analyzing the $\theta_{\mathrm{c.m.}}$ dependence on the CI n/p ratio will provide more information for revealing the reaction mechanism on the competition between the Coulomb and symmetry potentials. For $E_{\mathrm{beam}} = 35$ MeV/nucleon, the CI n/p ratios show a different $\theta_{\mathrm{c.m.}}$ dependence for the different forms of symmetry potential. In case of $\gamma_i = 0.5$, the CI n/p ratios slightly increase as a function of $\theta_{\mathrm{c.m.}}$. It is the result of the isospin asymmetry changing from $\delta_{\mathrm{proj}} = 0.10$ at the projectile region to $\delta_{\mathrm{tar}} = 0.19$ at the target region since the single particle potentials of neutrons and protons are close, as shown in Fig. 2(b). However, in the case of $\gamma_i = 2.0$, the CI n/p ratios obviously decrease with $\theta_{\mathrm{c.m.}}$, and the CI n/p ratios at backward regions are smaller than that at forward regions. Furthermore, we also analyze the angular distributions of the CI n/p ratios at beam energy for 50 and 100 MeV/nucleon. The CI n/p ratios increase as the beam energy increases except for the CI n/p at forward regions and $\gamma_i = 0.5$. The increasing behavior of the CI n/p ratios as the beam energy increases are from the enhancement of the symmetry potential at larger compressed density, which can be achieved with higher beam energies. However, CI n/p ratios at forward regions for $\gamma_i = 0.5$ show opposite behaviors; i.e., the CI n/p ratios decrease with the beam energy increasing. It is the effect of the finite size of the reaction systems. The final values of the CI n/p ratios from heavy ion collisions depend not only on the symmetry potential but also on the yield of nucleons for a finite reaction system. Since there are too many nucleons and LCPs emitted from the projectile for $\gamma_i = 0.5$ at $E_{\mathrm{beam}} = 100$ MeV/nucleon, the CI n/p ratios at forward regions tend to decrease to the initial N/Z value of projectile, $N/Z_{\mathrm{proj}} = 1.22$, which is obviously smaller than that obtained at 35 MeV/nucleon.

To check the smearing effects of impact parameters on the sensitivity of this observable to γ_i, calculations for $b = 4$ and 8 fm were also performed with IMQMD. The calculations show that the CI n/p ratio insignificantly depends on the impact parameters from $b = 4$ to 8 fm at beam energies of 35, 50, and 100 MeV/nucleon, because the value of the CI n/p ratio reflects the symmetry energy information of the reaction system which is not varied dramatically from $b = 4$ to 8 fm for ^{40}Ar + ^{197}Au. For its insensitivity to the changing of the impact parameter, the CI n/p ratio for mid-peripheral collisions is a valid probe for the symmetry energy.

Focusing on the anisotropy of angular distributions of the CI n/p ratios and its sensitivity to γ_i (or the slope of symmetry energy, $L = 3\rho_0 \frac{\partial S(\rho)}{\partial \rho}|_{\rho_0}$), we analyzed $R_{\mathrm{iso1}} = R_{\mathrm{CI}n/p}(20^\circ)/R_{\mathrm{CI}n/p}(90^\circ)$ and $R_{\mathrm{iso2}} = R_{\mathrm{CI}n/p}(90^\circ)/R_{\mathrm{CI}n/p}(160^\circ)$, which makes the experimental discrimination easier, for $b = 6$ fm at different beam energies. The calculations show R_{iso1} increases by ~20% when γ_i varies from 0.5 to 1.5 for $E_{\mathrm{beam}} = 35$ MeV/nucleon (see Fig. 6). For R_{iso2}, which is constructed from the backward regions, its values weakly depend on the symmetry energy for the beam energies we studied. Similar behaviors have also been found for 50 and 100 MeV/nucleon. These calculations illustrate that R_{iso1} is strongly correlated to the stiffness of the symmetry energy, and it would be helpful for us to extract the information of the symmetry energy and to understand the reaction mechanism as well as the spectra of CI n/p ratios if more complete data are measured.

IV. SUMMARY

In summary, the semi-peripheral heavy ion collisions of ^{40}Ar + ^{197}Au at $E_{\mathrm{beam}} = 35$, 50, and 100 MeV/nucleon

were studied by means of the improved quantum molecular dynamics model (ImQMD05). The competition between the symmetry potential and the Coulomb potential is discussed for the asymmetric reaction system. The calculations show that the impacts of the competition between Coulomb and symmetry potentials on the heavy ion collision observables, CI n/p ratio, can be observed at the projectile and target regions. In the case of $\gamma_i = 2.0$, the yields of protons are larger than for neutrons in the target region for beam energy at 35 MeV/nucleon due to its stronger Coulomb potential and weaker symmetry potential. As the beam energy increases up to 100 MeV/nucleon, the reaction is more violent and a larger part of the colliding system is dissociated into gases (nucleons and light particles), and thus more neutrons originally bound in the system are released and outnumber the protons. For $\gamma_i = 0.5$, the yields of neutrons are obviously greater than that for protons due to their stronger symmetry potential at subsaturation density. The competition between the Coulomb and symmetry potentials causes the anisotropy of the angular distribution of the coalescence invariant n/p ratio, $R_{\rm iso1}$, which is accordingly sensitive to the stiffness of the symmetry energy as well as the values of the CI n/p ratio. For $\gamma_i = 2.0$, the CI n/p ratios decrease with angle increasing, and $R_{\rm iso1} = 1.14 \pm 0.01$. For $\gamma_i = 0.5$, the CI n/p ratios slightly increase with angle because the single particle potential felt by the proton is close to that of the neutron, and $R_{\rm iso1} = 0.94 \pm 0.01$. The values of $R_{\rm iso1}$ increase by ~20% when γ_i varies from 0.5 ($L = 51$ MeV) to 1.5 ($L = 104$ MeV). The sensitivity of $R_{\rm iso1}$ to γ_i remains at all the beam energies we studied. It is of high interest to measure the isospin composition of the light particles over a wide angular range in further experiments at Fermi energies to gain comprehensive understanding on the reaction mechanism as well as on the symmetry energy behavior at subsaturation densities, and the symmetry energy in warm dilute matter.

ACKNOWLEDGMENTS

This work was supported by the National Key Basic Research Development Program of China under Grant No. 2013CB834404, the National Natural Science Foundation of China under Grants No. 11475262, No. 11275052, No. 11422548, No. 11375062, No. 11375094, and No. 11365004, and CUSTIPEN (China-US Theory Institute for Physics with Exotic Nuclei) under Department of Energy Grant No. DE-FG02-13ER42025. One of the authors, Y. X. Zhang, thanks Professor J. R. Stone for helpful discussions on the symmetry energy in nuclei.

[1] B. A. Brown, Phys. Rev. Lett. **85**, 5296 (2000).
[2] B. A. Li, L. W. Chen, and C. M. Ko, Phys. Rep **464**, 113 (2008).
[3] M. B. Tsang, W. A. Friedman, C. K. Gelbke, W. G. Lynch, G. Verde, and H. S. Xu, Phys. Rev. Lett. **86**, 5023 (2001).
[4] H.-Y. Wu *et al.*, Phys. Lett. B **538**, 39 (2002).
[5] M. B. Tsang *et al.*, Phys. Rev. Lett. **92**, 062701 (2004).
[6] L. W. Chen, C. M. Ko, and B.-A. Li, Phys. Rev. Lett. **94**, 032701 (2005).
[7] T. X. Liu *et al.*, Phys. Rev. C **76**, 034603 (2007).
[8] Z. Y. Sun *et al.*, Phys. Rev. C **82**, 051603(R) (2010).
[9] J. Rizzo, M. Colonna, V. Baran, M. Di Toro, H. H. Wolter, and M. Zielinska-Pfabe, Nucl. Phys. A **806**, 79 (2008).
[10] B. A. Li, L. W. Chen, G. C. Yong, and W. Zuo, Phys. Lett. B **634**, 378 (2006).
[11] M. A. Famiano *et al.*, Phys. Rev. Lett. **97**, 052701 (2006).
[12] Yingxun Zhang, P. Danielewicz, M. Famiano, Z. Li, W. G. Lynch, and M. B. Tsang, Phys. Lett. B **664**, 145 (2008).
[13] M. B. Tsang, Yingxun Zhang, P. Danielewicz, M. Famiano, Zhuxia Li, W. G. Lynch, and A. W. Steiner, Phys. Rev. Lett. **102**, 122701 (2009).
[14] S. Kumar, Y. G. Ma, G. Q. Zhang, and C. L. Zhou, Phys. Rev. C **84**, 044620 (2011).
[15] Y. Zhang, D. D. S. Coupland, P. Danielewicz, Z. X. Li, H. Liu, F. Lu, W. G. Lynch, and M. B. Tsang, Phys. Rev. C **85**, 024602 (2012).
[16] Y. X. Zhang, M. B. Tsang, Z. X. Li, and H. Liu, Phys. Lett. B **732**, 186 (2014).
[17] Wen-Jie Xie, Jun Su, Long Zhu, and Feng-Shou Zhang, Phys. Rev. C **88**, 061601(R) (2013).
[18] J. Rizzo, M. Colonna, M. Di Toro, and V. Greco, Nucl. Phys. A **732**, 202 (2004).
[19] Gao-Chan Yong, Bao-An Li, Lie-Wen Chen, and Xun-Chao Zhang, Phys. Rev. C **80**, 044608 (2009).
[20] Z. Kohley *et al.*, Phys. Rev. C **82**, 064601 (2010).
[21] V. Giordano, M. Colonna, M. Di Toro, V. Greco, and J. Rizzo, Phys. Rev. C **81**, 044611 (2010).
[22] M. D. Cozma, Phys. Lett. B **700**, 139 (2011).
[23] Yongjia Wang, Chenchen Guo, Qingfeng Li, Hongfei Zhang, Y. Leifels, and W. Trautmann, Phys. Rev. C **89**, 044603 (2014).
[24] Zhigang Xiao, Bao-An Li, Lie-Wen Chen, Gao-Chan Yong, and Ming Zhang, Phys. Rev. Lett. **102**, 062502 (2009).
[25] Zhao-Qing Feng and Gen-Ming Jin, Phys. Lett. B **683**, 140 (2010).
[26] Yuan Gao, G. C. Yong, Yongjia Wang, Q. Li, and W. Zuo, Phys. Rev. C **88**, 057601 (2013).
[27] Jun Hong and P. Danielewicz, Phys. Rev. C **90**, 024605 (2014).
[28] Z. G. Xiao *et al.*, Eur. Phys. J. A **50**, 37 (2014).
[29] M. Warda, X. Vinas, X. Roca-Maza, and M. Centelles, Phys. Rev. C **81**, 054309 (2010).
[30] L. W. Chen, Che Ming Ko, Bao-An Li, and Jun Xu, Phys. Rev. C **82**, 024321 (2010).
[31] M. K. Gaidarov, A. N. Antonov, P. Sarriguren, and E. M. deGuerra, Phys. Rev. C **85**, 064319 (2012).
[32] A. Carbone, G. Coló, A. Bracco, L.-G. Cao, P. F. Bortignon, F. Camera, and O. Wieland, Phys. Rev. C **81**, 041301(R) (2010).
[33] O. Wieland *et al.*, Phys. Rev. Lett. **102**, 092502 (2009).
[34] J. Piekarewicz, Phys. Rev. C **83**, 034319 (2011).
[35] P. Danielewicz and J. Lee, Nucl. Phys. A **818**, 36 (2009).
[36] Jianmin Dong, Wei Zuo, and Jianzhong Gu, Phys. Rev. C **87**, 014303 (2013).
[37] A. W. Steiner and S. Gandolfi, Phys. Rev. Lett. **108**, 081102 (2012).
[38] Kentaro Takami, Luciano Rezzolla, and Luca Baiotti, Phys. Rev. Lett. **113**, 091104 (2014).
[39] M. B. Tsang *et al.*, Phys. Rev. C **86**, 015803 (2012).
[40] J. M. Lattimer and A. W. Steiner, Eur. Phys. J. A **50**, 40 (2014).

[41] E. De Filippo *et al.*, Phys. Rev. C **86**, 014610 (2012); **71**, 044602 (2005).
[42] S. Hudan *et al.*, Phys. Rev. C **86**, 021603 (2012).
[43] F. Amorini *et al.*, Phys. Rev. Lett. **102**, 112701 (2009).
[44] R. S. Wang *et al.*, Phys. Rev. C **89**, 064613 (2014).
[45] P. Russotto *et al.*, Phys. Rev. C **81**, 064605 (2010).
[46] Yingxun Zhang and Zhuxia Li, Phys. Rev. C **71**, 024604 (2005).
[47] J. Colin *et al.*, Phys. Rev. C **67**, 064603 (2003).
[48] Y. Zhang and Z. Li, Phys. Rev. C **74**, 014602 (2006).
[49] Y. Zhang, Z. Li, and P. Danielewicz, Phys. Rev. C **75**, 034615 (2007).
[50] J. Aichelin, A. Rosenhauer, G. Peilert, H. Stoecker, and W. Greiner, Phys. Rev. Lett. **58**, 1926 (1987).
[51] Y. X. Zhang, Z. X. Li, C. S. Zhou, and M. B. Tsang, Phys. Rev. C **85**, 051602 (2012).
[52] V. Baran, M. Colonna, and M. Di Toro, Nucl. Phys. A **730**, 329 (2004).
[53] B. A. Li, C. M. Ko, and Z. Ren, Phys. Rev. Lett. **78**, 1644 (1997).
[54] R. Nebauer *et al.*, Nucl. Phys. A **658**, 67 (1999).
[55] D. D. S. Coupland, M. Youngs, W. G. Lynch, M. B. Tsang, Z. Chajecki, Y. X. Zhang, M. A. Famiano, T. K. Ghosh, B. Giacherio, M. A. Kilburn, Jenny Lee, F. Lu, P. Russotto, A. Sanetullaev, R. H. Showalter, G. Verde, and J. Winkelbauer, arXiv:1406.4546.
[56] B. A. Li, P. Danielewicz, and W. G. Lynch, Phys. Rev. C **71**, 054603 (2005).